Biophysical Characterization of Human XRCC1 and Its Binding to Damaged and Undamaged DNA †

ARTICLE *in* BIOCHEMISTRY · JANUARY 2005

Impact Factor: 3.02 · DOI: 10.1021/bi048615m · Source: PubMed

6 AUTHORS, INCLUDING:

Feridoun Karimi-Busheri
Erciyes Üniversitesi and university of alberta
40 PUBLICATIONS **2,041** CITATIONS
SEE PROFILE

Mesfin Fanta
Cross Cancer Institute
12 PUBLICATIONS **199** CITATIONS
SEE PROFILE

Carol E Cass
University of Alberta
304 PUBLICATIONS **11,466** CITATIONS
SEE PROFILE

Michael Weinfeld
University of Alberta
146 PUBLICATIONS **6,254** CITATIONS
SEE PROFILE

Biophysical Characterization of Human XRCC1 and Its Binding to Damaged and Undamaged DNA†

Rajam S. Mani,*,‡ Feridoun Karimi-Busheri,‡ Mesfin Fanta,‡ Keith W. Caldecott,§ Carol E. Cass,‡ and Michael Weinfeld*,‡

Department of Experimental Oncology, Cross Cancer Institute, and Department of Oncology, University of Alberta, Edmonton, Alberta T6G 1Z2, Canada, and Genome Damage and Stability Centre, University of Sussex, Science Park Road, Falmer, Brighton BN1 9RQ, U.K.

Received June 30, 2004; Revised Manuscript Received September 28, 2004

ABSTRACT: The human DNA repair protein, hXRCC1, which is required for DNA single-strand break repair and genetic stability was produced as a histidine-tagged polypeptide in *Escherichia coli*, purified by affinity chromatography, and subjected to sedimentation and spectroscopic analyses. This study represents the first biophysical examination of full-length XRCC1. Sedimentation equilibrium measurements indicated that hXRCC1 exists as a monomer at lower protein concentrations but forms a dimer at higher protein concentrations with a K_d of 5.7×10^{-7} M. The size and shape of hXRCC1 in solution were determined by analytical ultracentrifugation studies. The protein exhibited an intrinsic sedimentation coefficient, $s^0_{20,w}$, of 3.56 S and a Stokes radius, R_s, of 44.5 Å, which together with the M_r of 68000 suggested that hXRCC1 is a moderately asymmetric protein with an axial ratio of 7.2. Binding of model ligands, representing single-strand breaks with either a nick or a single nucleotide gap, quenched protein fluorescence, and binding affinities and stoichiometries were determined by carrying out fluorescence titrations as a function of ligand concentration. XRCC1 bound both nicked and 1 nucleotide-gapped DNA substrates tightly in a stoichiometric manner (1:1) with K_d values of 65 and 34 nM, respectively. However, hXRCC1 exhibited lower affinities for a duplex with a 5 nucleotide gap, the intact duplex with no break, and a single-stranded oligonucleotide with K_d values of 215, 230, and 260 nM, respectively. Our results suggest that hXRCC1 exhibits preferential binding to DNA with single-strand breaks with a gap size of <5 nucleotides.

The X-ray repair cross-complementing group 1 (*XRCC1*) gene was the first mammalian gene isolated that affects cellular sensitivity to ionizing radiation (*1*). The 633 amino acid protein encoded by the human *XRCC1* gene is required for maintenance of genome stability (*2*) and efficient repair of oxidative DNA base damage and DNA single-strand breaks by the base excision repair (BER)[1] and single-strand break repair (SSBR) pathways, respectively (*3*, *4*). Both pathways are essential for the repair of DNA damage inflicted by ionizing radiation and alkylating agents, including many chemotherapeutic drugs currently in use (*5*). Other results support a role for XRCC1 protein in genetic stability in noncycling and postmitotic stages of the cell cycle (*6*).

Current evidence strongly indicates that XRCC1 functions as a chaperone or scaffolding protein capable of interacting with several proteins participating in different repair pathways. It forms complexes with poly(ADP-ribose) polymerase (PARP) (*7*, *8*), DNA polymerase β (*9*, *10*), DNA ligase III (*11*), polynucleotide kinase (*12*), human AP endonuclease (*13*), and proliferating cell nuclear antigen (PCNA) at DNA replication foci to facilitate SSBR at S phase (*14*).

Structural analysis of XRCC1 focused initially on one of its BRCA1 carboxyl-terminal (BRCT) conserved domains. Several other DNA repair and cell cycle regulator proteins contain BRCT domains (*15*, *16*). The first three-dimensional structure of a BRCT domain was obtained for the C-terminal region (residues 538−633) of XRCC1 (*17*) containing the BRCT II domain. This structure provided a framework for modeling other BRCT domains and interactions between BRCT domains on different proteins, including the physical association between XRCC1 and DNA ligase IIIα (*11*, *18*, *19*). The DNA binding and polymerase β binding sites of XRCC1 have been mapped to its N-terminal domain (*9*, *20*). The NMR solution structure of this domain, located within residues 84−183, indicated preferential binding to a DNA ligand bearing a single-strand break (*20*).

The contact regions of hXRCC1 with a number of other proteins have also been determined. These include PARP 1 and 2, OGG1 glycosylase and AP endonuclease I, which can bind to the BRCT I domain (*21*, *22*), and the forkhead-associated domain of polynucleotide kinase, which binds

† This work was supported by the Canadian Institutes of Health Research, the Alberta Cancer Board, the Alberta Cancer Foundation, the Alberta Heritage Foundation for Medical Research, and the National Cancer Institute of Canada. C.E.C. is Canada Research Chair in Oncology.

* To whom correspondence should be addressed at the Department of Experimental Oncology, Cross Cancer Institute, 11560 University Ave., Edmonton, Alberta T6G 1Z2, Canada. Phone: 780-432-8438. Fax: 780-432-8428. E-mail: mweinfel@ualberta.ca and rajam.mani@cancerboard.ab.ca.

‡ Department of Experimental Oncology, Cross Cancer Institute, and Department of Oncology, University of Alberta.

§ Genome Damage and Stability Centre, University of Sussex.

[1] Abbreviations: hXRCC1, human X-ray repair cross-complementing group 1; BER, base excision repair; SSBR, single-strand break repair; PARP, poly(ADP-ribose) polymerase; Tris, tris(hydroxymethyl)aminomethane; EDTA, ethylenediaminetetraacetic acid; SDS, sodium dodecyl sulfate; PAGE, polyacrylamide gel electrophoresis; Hepes, 4-(2-hydroxyethyl)-1-piperazineethanesulfonic acid; nt, nucleotide.

10.1021/bi048615m CCC: $27.50
Published on Web 12/02/2004

within a C-terminal domain (residues 402−529) of hXRCC1 (*23*). This latter binding is greatly stimulated by casein kinase 2-mediated phosphorylation of XRCC1 (*23*).

Despite the fact that several peptide domains have been identified and two of these have been characterized at the molecular level, there are still many physical properties of hXRCC1 that remain to be resolved. This work represents the first biophysical examination of full-length hXRCC1 in solution. We carried out detailed hydrodynamic studies to establish its oligomeric state in nondenaturing medium, mimicking its cellular milieu. Our data indicate that hXRCC1, at low protein concentration, exists as a monomer and is moderately asymmetric but at higher concentrations exists predominantly as a dimer. The hXRCC1 protein exhibited strong affinity for DNA with single-strand breaks (nick or 1 nucleotide gap) with 1:1 protein:ligand binding stoichiometry.

MATERIALS AND METHODS

Expression of His-Tagged XRCC1 in Escherichia coli. The pET16BXH construct (*24*) carrying a histidine (His10) tag at the C-terminus of human XRCC1 was transfected into host *E. coli* strain BL21(DE3) (Novagen). The bacteria were grown at 37 °C to an OD_{600} of 0.6 in 60 mL of LB medium containing ampicillin at a concentration of 100 μg/mL and then kept at 4 °C overnight. The pelleted cells were used to inoculate 4 L of LB media and then grown at 37 °C to an OD_{600} of 0.6. XRCC1 expression was induced at 37 °C for 90 min by addition of isopropyl 1-thio-β-D-galactopyranoside (Sigma, St. Louis, MO) to a final concentration of 1 mM. After the cells were harvested by centrifugation at 5000*g* at 4 °C for 10 min, the cells were resuspended in 40 mL of ice-cold sonication buffer (50 mM Hepes−NaOH, pH 8.0, 0.5 M NaCl, 0.1 mM EDTA, 10% glycerol), quick frozen in liquid nitrogen, and thawed on ice followed by addition of imidazole, dithiothreitol, and phenylmethanesulfonyl fluoride to a final concentration of 1 mM for each reagent. The bacteria were disrupted by sonication on ice, and the soluble fraction was obtained by centrifugation at 10000*g* for 20 min.

Purification of His-Tagged XRCC1 Protein. Recombinant XRCC1 was isolated from the supernatant using ProBond nickel-chelating resin (Invitrogen Life Technologies, Carlsbad, CA) according to the manufacturer's instructions and as described previously (*24*). Briefly, supernatant from 2 L of culture was mixed with 3 mL of nickel-charged affinity resin and stirred on ice for approximately 1 h. The slurry was loaded into a 5 mL column at a flow rate of 3 mL/min, and the flow-through (40 mL) was collected. The column was washed with 20 mL of sonication buffer and 30 mL of wash buffer (50 mM Hepes−NaOH, pH 7.0, 0.1 M NaCl, 0.1 mM EDTA, 1 mM dithiothreitol, 10% glycerol) containing 40 mM imidazole, pH 8.0, at a flow rate of 0.5 mL/min. The column was washed further with 15 mL of wash buffer containing 80 mM imidazole, and the bound protein was subsequently eluted with 15 mL of wash buffer containing 250 mM imidazole in 1.5 mL fractions. The protein purity was assessed by electrophoresis of 10 μL of each fraction on a 10% SDS−polyacrylamide gel and Coomassie Blue staining. The desired protein concentration and buffer exchange (50 mM Tris-HCl, pH 7.5, 100 mM NaCl, 5 mM $MgCl_2$, and 1 mM dithiothreitol) were achieved by using a 30 kDa cutoff Millipore ultrafree concentrator.

Hydrodynamic Studies. Fringe counts were performed using a Beckman XLI analytical ultracentrifuge and double-sector capillary synthetic boundary sample cells as described by Babul and Stellwagen (*25*). Prior to ultracentrifugation, protein samples were dialyzed for 48 h in 50 mM Tris-HCl buffer (pH 7.5), 100 mM NaCl, 5 mM $MgCl_2$, and 1 mM dithiothreitol. The absorbance of each sample was measured using 1.0 cm path length cuvettes. Samples (150 μL) were loaded into one sector of the sample cell, and 400 μL of the dialysate was loaded into the other sector. Runs were performed at 8000 rpm, and scans were taken when fringes were resolved across the boundary region between protein solution and solvent. The number of fringes produced across the boundary was measured and converted to concentration using an average increment of 3.31 fringes mg^{-1} mL^{-1}. From a plot of the number of fringes versus optical density, a value of 7.90 was established as the extinction coefficient, $\epsilon^{1\%}_{1cm,280nm}$, for hXRCC1.

Sedimentation Velocity Measurements. Sedimentation velocity experiments were carried out at 20 °C and 50000 rpm using the XLI analytical ultracentrifuge and absorption optics following the procedures described by Laue and Stafford (*26*) and as also outlined in the instruction manual (Spinco Business Center of Beckman Instruments, Inc., Palo Alto, CA). Four hundred microliters of sample solution and 400 μL of dialysate were loaded into two-sector CFE centerpiece sample cells containing sapphire windows. Runs were performed for 4 h during which time a minimum of 30 scans were taken. The sedimentation velocity data were analyzed according to Williams et al. (*27*) to determine the sedimentation coefficient, *s*. The intrinsic sedimentation coefficient, $s^0_{20,w}$, which represents the sedimentation coefficient corrected to water at 20 °C, was then calculated from the observed *S* value as described by Laue et al. (*28*).

Sedimentation Equilibrium Studies. Sedimentation equilibrium experiments were carried out at 5 °C using absorption optics. Samples (110 μL) were loaded into six-sector CFE cells, allowing three concentrations of sample to be run simultaneously. Runs were performed at 9000 and 11000 rpm, and each speed was maintained until there was no significant difference in scans taken 2 h apart to ensure equilibrium was achieved. The sedimentation equilibrium data were evaluated with the Nonlin analysis program using a nonlinear least-squares curve-fitting algorithm (*29*). The program Sednterp (Sedimentation Interpretation Program, version 1.01) was employed to calculate the partial specific volume of the protein from the amino acid composition using the method of Cohn and Edsall (*30*).

Hydrodynamic Calculations and Ellipsoid Modeling. The observed sedimentation coefficient, *s*, determined from sedimentation velocity data will correspond to the maximum *S* value that can be obtained for the given molecular mass of the protein and correspondingly the protein would have the minimum frictional coefficient, f_0. Translational frictional ratios (f/f_0) were calculated from the experimental Stokes radius obtained from sedimentation velocity experiments ($R_{s,sed}$) according to Mani and Kay (*31*). The frictional ratio f/f_0, which is equivalent to $S_{max}/s_{20,w}$, indicates the maximum shape asymmetry of the protein. The total shape asymmetry depends on two factors, a geometrical shape asymmetry and expansion due to hydration. A globular protein with different ellipsoid shapes can be modeled from f/f_0 or f/f_{shape} values

Table 1: Schematic Representation of Model Substrates

Model Substrate	Oligonucleotide Sequences
Nick	5′-ATTACGAATGCCCACACCGCCGGCGCCCACCACCACTAGCTGGCC-3′ 3′-TAATGCTTACGGGTGTGGCGGCCGCGGGTGGTGGTGATCGACCGG-5′
1 nt-Gap	5′-ATTACGAATGCCCACACCGC GGCGCCCACCACCACTAGCTGGCC-3′ 3′-TAATGCTTACGGGTGTGGCGGCCGCGGGTGGTGGTGATCGACCGG-5′
1 nt-Gap (5′-P)	5′-ATTACGAATGCCCACACCGC GGCGCCCACCACCACTAGCTGGCC-3′ 3′-TAATGCTTACGGGTGTGGCGGCCGCGGGTGGTGGTGATCGACCGG-5′
5 nt-Gap	5′-ATTACGAATGCCCACACCGC CCCACCACCACTAGCTGGCC-3′ 3′-TAATGCTTACGGGTGTGGCGGCCGCGGGTGGTGGTGATCGACCGG-5′
Single	5′-ATTACGAATGCCCACACCGCCGGCGCCCACCACCACTAGCTGGCC-3′
Duplex	5′-ATTACGAATGCCCACACCGCCGGCGCCCACCACCACTAGCTGGCC-3′ 3′-TAATGCTTACGGGTGTGGCGGCCGCGGGTGGTGGTGATCGACCGG-5′

(*28*), using the software program Sednterp 1.01, in which the semimajor to semiminor (*a*/*b*) axial ratio of a prolate or oblate ellipsoid of revolution is determined using the respective power series approximation of the tabulated data for *a*/*b* as a function of ($f/f_0 - 1$) or ($f/f_{shape} - 1$) for each ellipsoid. To calculate f/f_{shape} using Sednterp, the δ value, which corresponds to hydration in grams of water per gram of protein, was based on the amino acid composition of XRCC1 (*32*). The Sednterp program provides a graphical presentation of the hydrodynamic model from the volume of an ellipsoid ($^4/_3\pi ab^2$), which is equivalent to the volume of the hydrated protein.

Fluorescence Studies. Steady-state fluorescence spectra were measured at room temperature on a Perkin-Elmer LS-55 spectrofluorometer (Freemont, CA) with 5 nm spectral resolution for excitation and emission using 0.1−0.2 μM solutions of purified recombinant hXRCC1. Protein fluorescence was excited at 295 nm, and fluorescence emission spectra were recorded in the 300−400 nm range; changes of fluorescence were usually monitored at the emission maximum (326 nm). In studying the effects of DNA ligands (Table 1) on protein fluorescence intensities, additions to hXRCC1 samples were made from ligand stock solutions, keeping the protein dilution below 3%, and fluorescence intensities were corrected for dilution factors. Background quenching, if present (<2%), was eliminated by subtracting the signal obtained from a buffer solution that contained the appropriate quantity of ligand. The total absorption of the enzyme samples was kept below 0.05 at 295 nm. The oligonucleotides used to generate the XRCC1 ligands were synthesized by UCDNA Services (University of Calgary, Calgary, Alberta, Canada).

Circular Dichroism Spectroscopy. Circular dichroism (CD) measurements were performed in an Olis DSM 17CD spectropolarimeter (Bogart, GA) calibrated with a 0.06% solution of ammonium *d*-camphor-10-sulfonate. The temperature in the sample chamber was maintained at 20 °C. Each sample was scanned five times, and baseline buffer spectra were subtracted from protein sample spectra before molar ellipticities were calculated. To obtain spectra in the far-UV region, the cell path length was 0.02 cm and the protein concentration was around 0.5 mg/mL. The CD spectra were analyzed for secondary structures according to Compton and Johnson (*33*).

RESULTS

Expression and Purification of XRCC1. Active recombinant human XRCC1 was produced in *E. coli* and purified using immobilized metal chelate affinity chromatography according to Caldecott et al. (*24*). The SDS gel, stained with silver nitrate (Figure 1), indicated purification to near homogeneity. Despite having a molecular mass of approximately 70000 Da, based on its amino acid sequence, the protein migrated with an apparent molecular mass of ~85000 Da, consistent with the published values for XRCC1 (*24*, *34*). The UV absorption spectrum of the His-tagged hXRCC1 exhibited an absorption maximum at 279, characteristic of tyrosine residues, and a shoulder around 290 nm, characteristic of tryptophan residues (data not shown). The 280/260 and 280/290 absorbance values were 1.72 and 1.5, respectively. Protein concentrations were determined using an extinction coefficient, $\epsilon^{1\%}_{280nm}$, of 7.9, a value that was established by the refractometric method of Babul and Stellwagen (*25*).

Sedimentation Velocity Studies. In the analytical ultracentrifuge hXRCC1, which has a sequence molecular mass of 69525 Da, sedimented as a single peak with an intrinsic $s^0_{20,w}$ value of 3.56, suggesting that it must be moderately asymmetric, since a globular protein like bovine serum albumin with a molecular mass of 66000 Da sediments much faster

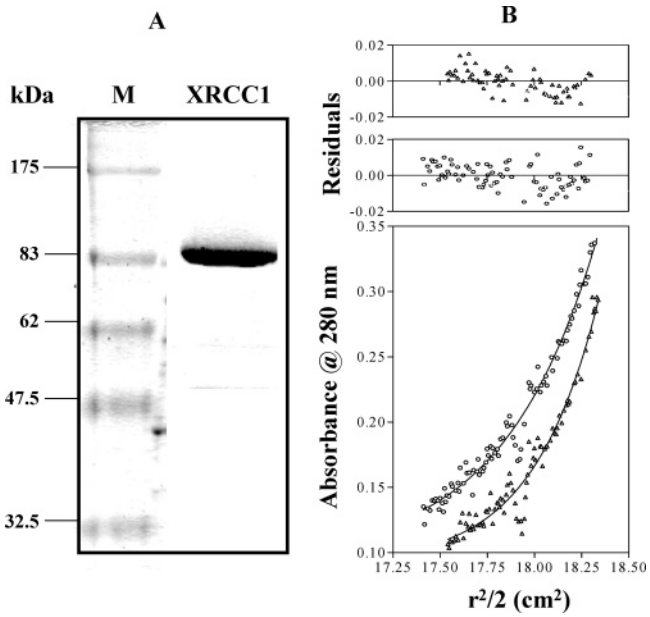

FIGURE 1: (A) Electrophoresis of purified hXRCC1 in a 10% SDS−polyacrylamide gel. The left lane shows size markers in kDa. (B) Sedimentation equilibrium profiles for hXRCC1 obtained at 14000 rpm (circles) and 16000 rpm (triangles) at 5 °C in 50 mM Tris-HCl, pH 7.5, 100 mM NaCl, 5 mM $MgCl_2$, and 1 mM dithiothreitol for 48 h. The loading protein concentration was 0.28 mg/mL. Global nonlinear regression fitting of both data sets was performed for a single component system, and the solid lines denote the fitted curves. The residuals for each fit are shown in the upper panels above the absorbance vs radial distribution profiles.

with an $s^0_{20,w}$ value of 4.6. The effect of varying protein concentration on $s_{20,w}$ was studied to ascertain if hXRCC1 had a tendency to aggregate at a higher concentration. The weight-average sedimentation coefficient increased in concert with increasing protein concentration, suggesting that the subunits are in a rapidly reversible equilibrium between monomeric and oligomeric forms. The sedimentation boundary profiles obtained at different concentrations were unimodal, whereas a rapidly reversible system in which the only oligomers formed are larger than dimers would be expected to exhibit bimodality (*35*−*38*). Hence, the observed boundary profiles suggested that the subunits were either in a rapidly reversible equilibrium between monomers and dimers or between monomers, dimers, and higher oligomers. The apparent $s_{20,w}$ values obtained at 0.33 and 0.8 mg/mL were 3.73 and 3.92, respectively. This is expected for a polymerizing system, since the fraction of the subunits polymerized increases with increasing protein concentration in accordance with the law of mass action, leading to increased observed $s_{20,w}$ values.

Sedimentation Equilibrium Studies. To understand the nature of this polymerization of hXRCC1, sedimentation equilibrium experiments were performed, since this technique allows direct determination of absolute molecular mass, independent of protein shape. From a single equilibrium ultracentrifugation run, the weight-average molecular mass can be determined as a function of protein concentration at each point in the cell, and from these data one can determine both the stoichiometry and equilibrium constants for the various species that are present. Sedimentation equilibrium runs were performed at two different speeds for three initial loading concentrations of hXRCC1, and each data set was analyzed individually (Figure 2). When a model for a single species was used, apparent molecular masses between those for a monomer and a dimer were observed (116000−125000 Da), and the oligomer values ranged from 1.65 to 1.80, using a value of 69525 Da for the monomer. The data demonstrate that hXRCC1 self-associated to a higher order species approximating a dimer at 5 °C. Sedimentation equilibrium data fit well to a monomer−dimer model and the weighted global fit (shown in Figure 2) gave a molecular mass of 120000 ± 5000 Da, suggesting that under these conditions hXRCC1 existed predominantly (86% of total) as a dimer. No improvement of fit was seen upon inclusion of other oligomeric species to the fitting model. Global fitting of all six data sets, using a reversibly associating monomer−dimer model, yielded a dissociation constant of 5.7×10^{-7} M for the XRCC1 dimer, which corresponds to a ΔG value of ~8.5 kcal/mol at 20 °C. A K_a value of 1.75×10^6 M^{-1} for the association constant indicates a fairly strong association between monomers to form dimers and is comparable to values quoted for other protein/protein complexes. For example, a ΔG value of 9.5 kcal/mol has been reported for the dissociation of the dimeric enzyme enolase (*39*).

We also carried out sedimentation equilibrium runs using an initial loading concentration of 0.28 mg/mL (4.0 μM) hXRCC1. Under this condition, the sedimentation data (Figure 1B) fit well to a single-species model with an apparent molecular mass of 68000 Da, implying that hXRCC1 was monomeric in solution at this low protein concentration, and the calculated M_r is in excellent agreement with the predicted M_r of the 633 amino acid polypeptide encoded by the sequenced cDNA for hXRCC1 and the additional 10 amino acids of the His tag of 69525.

Shape and Length. Since hXRCC1 exists as a monomer at lower protein concentrations, some idea of the shape of the hXRCC1 protein molecule can be obtained from the frictional ratio, f/f_0, which can be calculated from the intrinsic sedimentation coefficient, $s^0_{20,w}$, value, partial specific volume, and molecular mass (*31*). The calculated f/f_0 was equal to 1.38, assuming hydration of 0.44 g of H_2O/g based on amino acid composition (*32*). Assuming hXRCC1 to be a prolate ellipsoid, the value of f/f_0 yielded an apparent axial ratio, $a/b = 7.2$, where a and b are major and minor semidiameters, respectively (*40*, *41*). Figure 3 represents a graphical presentation of this model with the water of hydration as a separate layer obtained using the Sednterp software program (*28*). Alternatively, a rod-shaped model with length $2a$ and a volume equivalent to the prolate ellipsoid would have an axial ratio, i.e., length/diameter (L/d) of 8.7 (*41*). Hence, with either model, it is clear that hXRCC1 is a moderately asymmetric protein molecule.

The length of hXRCC1 can be calculated from its volume, which can be estimated (i) using the molecular mass, partial specific volume (determined from its amino acid composition), and water of hydration and (ii) assigning a model for its shape. For the ellipsoidal model with $a/b = 7.2$, the length is given by $2a$ and is 239.0 Å with a diameter of $2b = 31.90$ Å (*31*) and is in excellent agreement with the values obtained using the Sednterp program (Figure 3). If hXRCC1 is assumed to be a rod ($L/d = 8.7$), the values for d and L are 26.5 and 231.0 Å, respectively. Hence, the calculated dimensions of hXRCC1 in solution appear to approximate to 235 × 30 Å with an axial ratio of about 8:1, regardless of the model chosen.

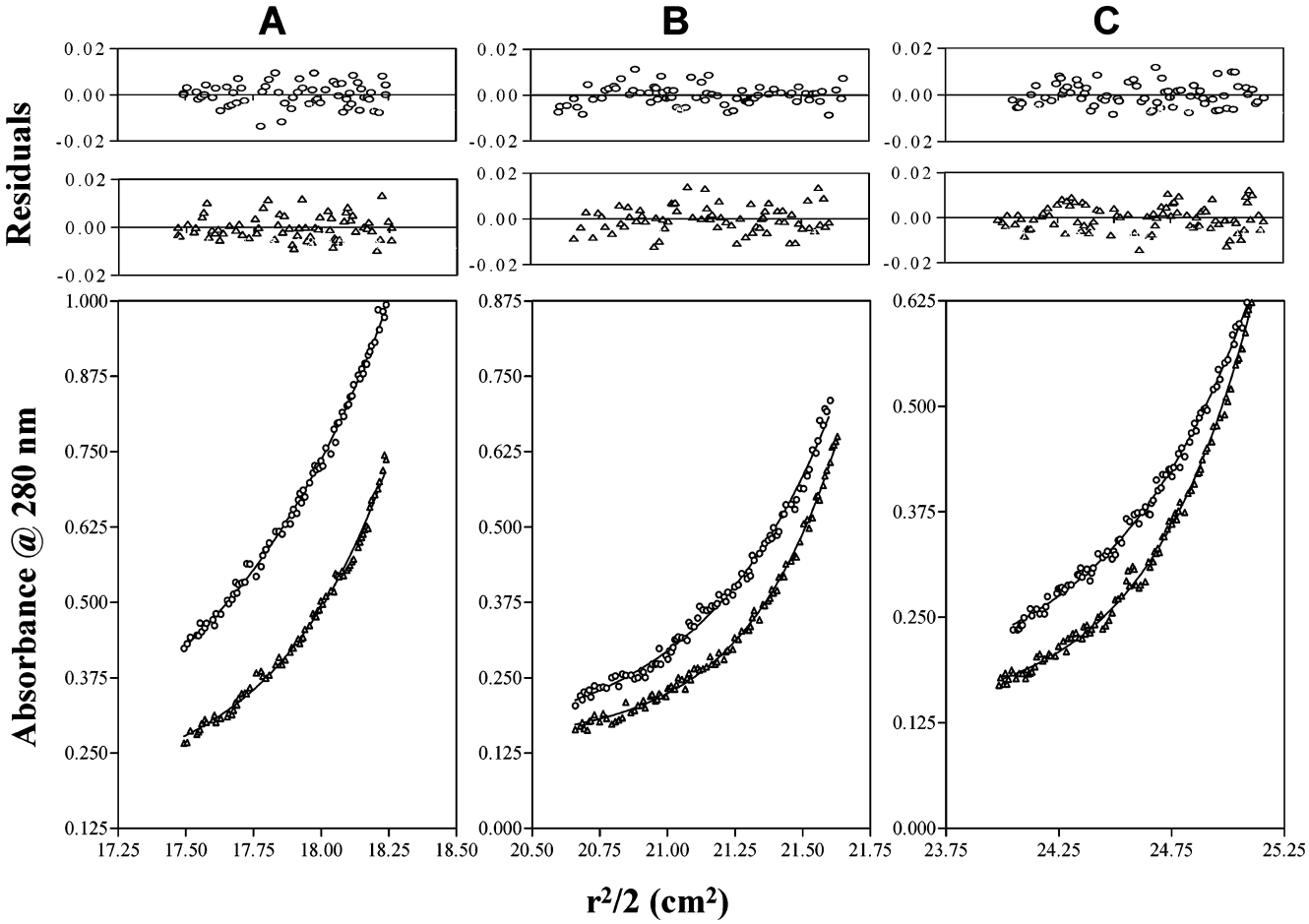

FIGURE 2: Sedimentation equilibrium profiles for hXRCC1 obtained at 9000 rpm (circles) and 11000 rpm (triangles) at 5 °C. The absorbance as a function of radial position for hXRCC1 is shown for the following initial loading concentrations: 1.2 mg/mL (A), 0.8 mg/mL (B), and 0.6 mg/mL (C). Global nonlinear regression fitting of all six data sets was performed for a monomer/dimer two-component system, and the solid lines denote the fitted curves. The residuals for each fit are shown in the upper panels above the absorbance vs radial distribution profiles.

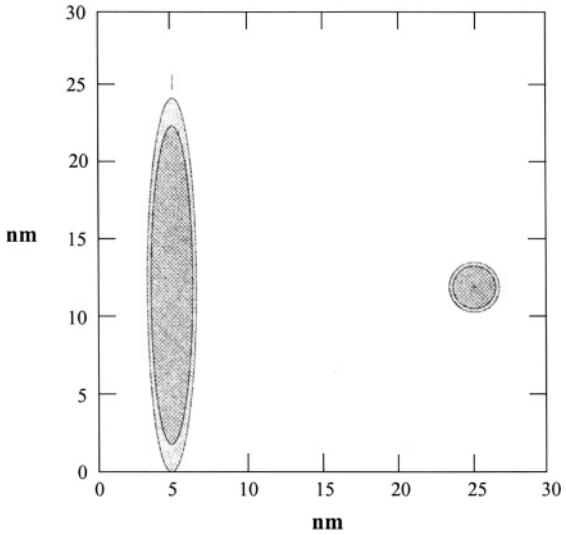

FIGURE 3: Hydrated prolate ellipsoid model for hXRCC1. The figure shows the size and shape (in nanometers) of the protein and the surrounding layer of hydration in a side view (left) and a view down the central axis (right), with the water of hydration displayed as a separate layer on the outside. Hydration expands the shape of the prolate model by 17.4%.

Fluorescence Spectroscopy. Although hXRCC1 has 6 tryptophans and 13 tyrosines, the observed fluorescence was due to tryptophan residues since the protein was excited at 295 nm. Fluorescence spectra of hXRCC1 were measured in Tris-HCl buffer, pH 7.5, in the absence and presence of 6 M guanidine hydrochloride (Gdn-HCl). In the absence of the denaturant, the emission maximum was at 326 ± 1 nm, and in 6 M Gdn-HCl, the emission maximum was red shifted to 353 ± 1 nm. These results indicated that the unfolding of hXRCC1 in 6 M Gdn-HCl exposed the partly buried tryptophan residues to a more polar environment.

We studied the effects of the binding of six model oligonucleotide substrates [i.e., a nicked duplex, a single nucleotide (1 nt) gapped duplex, a single nucleotide (1 nt) gapped duplex with a 5′-phosphate, a five nucleotide (5 nt) gapped duplex, an intact duplex with no breaks, and a single-stranded oligonucleotide; sequences provided in Table 1] to hXRCC1 by determining the response of its fluorescence to increasing concentrations of ligands. The hXRCC1−ligand interactions resulted in partial quenching of fluorescence with no change in emission maximum, which enabled determination of binding affinities (K_d) and stoichiometries by following fluorescence quenching (a measure of ligand binding) as a function of ligand concentration. A plot of the relative fluorescence intensity versus the concentration of 1 nt-gapped DNA is shown in Figure 4A (inset). The maximum quenching of fluorescence intensity observed at saturating concentration of the gapped DNA was taken as 1, and the observed quenching at different concentrations of gapped

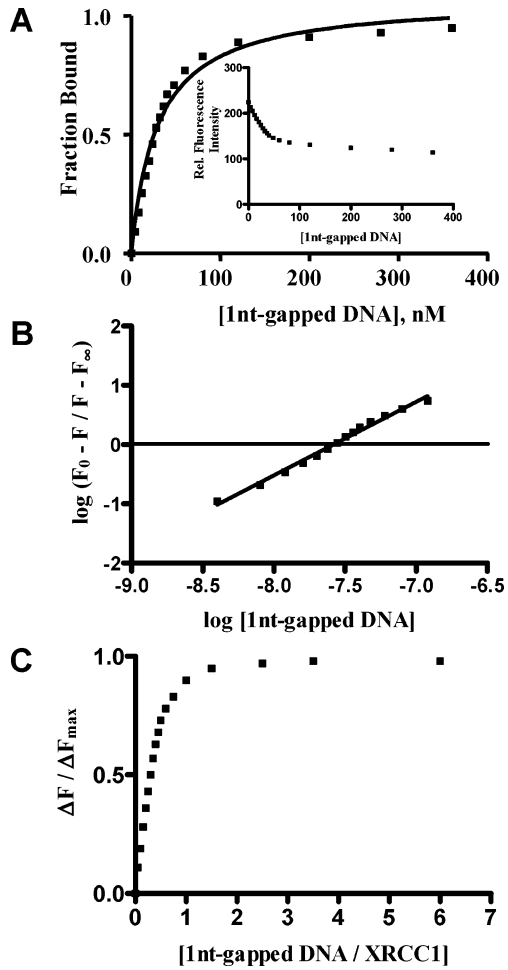

FIGURE 4: Fluorescence titration of hXRCC1 vs duplex with a single nucleotide gap. (A) hXRCC1 (78 nM) against gapped DNA in 50 mM Tris-HCl, pH 7.5, 100 mM NaCl, 5 mM $MgCl_2$, and 1 mM dithiothreitol. The protein was excited at 295 nm, and the fluorescence intensity was monitored at 326 nm (see inset). The fraction bound (i.e., relative fluorescence quenching) vs ligand concentration is plotted. (B) Sample plot of fluorescence data from titration with gapped DNA. F_0, F, and F_∞ are the relative fluorescence intensities at 326 nm of hXRCC1 alone, hXRCC1 in the presence of a given concentration of gapped DNA, and hXRCC1 saturated with gapped DNA, respectively. The plot is according to Chipman et al. (*52*). (C) The observed change in fluorescence intensity, ΔF, at a given ligand concentration divided by the maximum change at saturating ligand concentration, ΔF_{max}, is plotted against the molar ratio of ligand to protein.

DNA was plotted as the fraction bound versus gapped DNA concentration (Figure 4A). Nonlinear regression analysis (GraphPad Prism Software, San Diego, CA) of the binding data revealed unimodal binding with a K_d value of 34 ± 3 nM. In Figure 4B, $\log(F_0 - F)/(F - F_\infty)$ is plotted against log[1 nt-gapped DNA], where F_0, F, and F_∞ are the fluorescence intensities of solutions of enzyme alone, enzyme in the presence of various concentrations of gapped DNA, and enzyme saturated with gapped DNA, respectively. This plot yielded a slope of 1.10, indicating a 1:1 interaction between gapped DNA and hXRCC1. Since the protein bound the gapped DNA tightly, $\Delta F/\Delta F_{max}$ versus [1 nt-gapped DNA]/[XRCC1] was also plotted (*42*) to determine the binding stoichiometry, and as can be seen from Figure 4C, the ΔF value leveled off when the mole ratio was 1:1, taking the monomer molecular mass of 69525 Da for XRCC1.

The binding of hXRCC1 to nicked DNA, duplex, and the single-stranded oligonucleotide is shown in Figure 5. The K_d values obtained with all of the substrates are presented in Table 2. The affinities with which hXRCC1 bound these ligands were 1 nt-gapped DNA ∼ 1 nt-gapped (5′-P) > nicked DNA ≫ 5 nt-gapped DNA > intact duplex > single-stranded oligonucleotide. The values indicate that there is a substantial difference in binding affinity for damaged versus undamaged or single-stranded substrates. While the presence of a 5′-phosphate at a 1 nt gap had very little influence, widening the gap to five nucleotides reduced the affinity of the protein to the same level as the undamaged substrate. The binding stoichiometry determined for all of these substrates was also 1:1, suggesting XRCC1 binds its substrates in a stoichiometric manner.

In addition, we also determined the binding affinity of XRCC1 for 1 nt-gapped DNA in the presence of single-stranded oligonucleotide by fluorometric titration. For this experiment, we first added 0.5 μM single-stranded oligonucleotide (∼2 × K_d) to XRCC1, and the tryptophan emission intensity obtained at 326 nm in the presence of single-stranded oligonucleotide was taken as the control value. Quenching of the fluorescence intensity was then monitored as a function of the concentration of added 1 nt-gapped DNA to determine the binding affinity of the 1 nt-gapped DNA to XRCC1 in the presence of single-stranded oligonucleotide. The K_d value obtained in this instance was 55 ± 5 nM, suggesting that XRCC1 was capable of binding 1 nt-gapped DNA with high affinity in the presence of competing single-stranded oligonucleotide. On the other hand, the presence of 1 nt-gapped DNA (75 nM; ∼2 × K_d) interfered with the XRCC1−single-stranded oligonucleotide interaction. The K_d value obtained with the single-stranded oligonucleotide in this instance was ∼1 μM, indicating that the binding affinity was reduced approximately 4-fold compared with the value of 260 nM in the absence of competing 1 nt-gapped substrate.

Circular Dichroism Studies. Information concerning the secondary structure of hXRCC1 was obtained from far-UV−CD data, and a typical far-UV−CD spectrum of hXRCC1 is shown in Figure 6. hXRCC1 exhibited two large, negative CD bands centered around 208 and 218 nm, indicating the presence of α-helical organization. The observed molar ellipticities, $[\theta]_M$, at these two wavelengths were − 8700 ± 300 and −6100 ± 300 deg cm^2 dmol^{-1}, respectively. The CD spectra were analyzed according to the method of Compton and Johnson (*33*). The protein possessed ∼40% α-helix and ∼30% β-structure, and the remaining ∼30% represented random structure.

Since, hXRCC1 exhibited strong affinity for 1 nt-gapped and nicked DNA and significantly lower affinities for the intact duplex with no break and a single-stranded oligonucleotide, we studied the effect of 1 nt-gapped and nicked DNA on hXRCC1 protein conformation. It is evident from Figure 6 that the addition of 1 nt-gapped DNA induced a conformational change in hXRCC1; the molar ellipticity values $[\theta]_M$ at 208 and 218 nm were reduced to −7000 ± 300 and −5200 ± 300 deg cm^2 dmol^{-1}, respectively. Analysis of the CD data indicated an increase in α-helical content accompanied by a decrease in β-structure, and the calculated values were α-helix (45%) and β-structure (25%) and the random structure corresponded to 30%. The binding

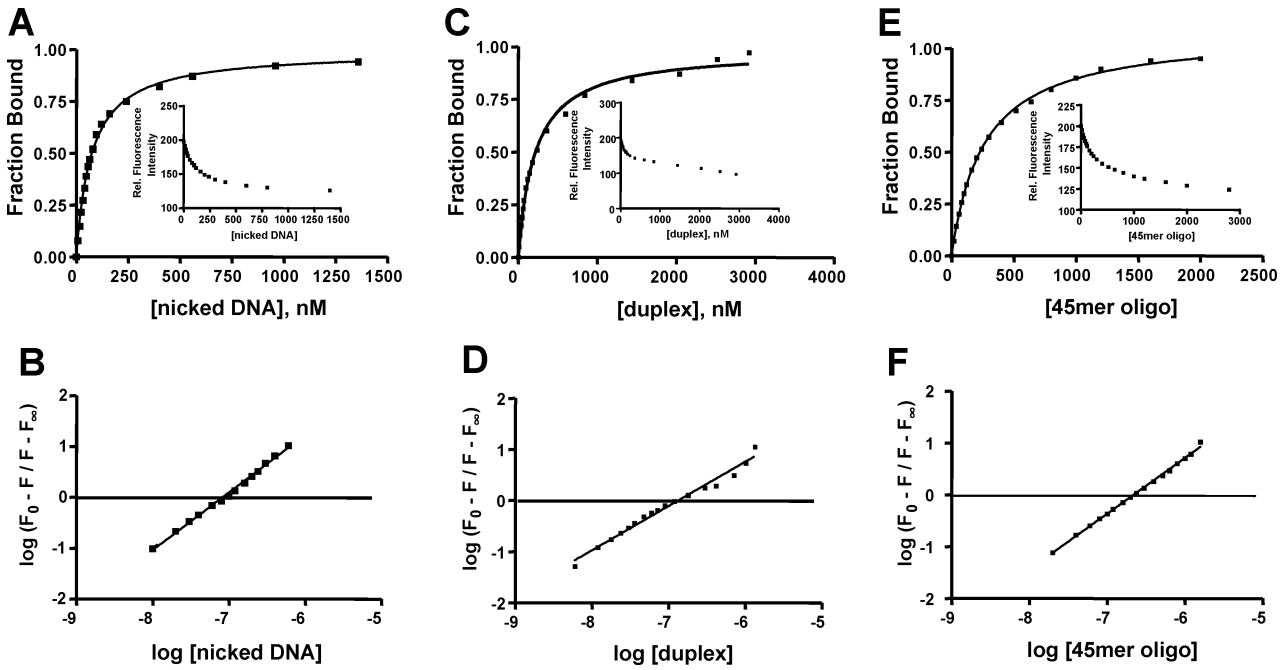

FIGURE 5: Fluorescence titration of hXRCC1 with DNA ligands: (A, B) hXRCC1 (78 nM) vs nicked DNA; (C, D) hXRCC1 (95 nM) vs duplex; (E, F) hXRCC1 (95 nM) vs single-stranded oligonucleotide.

Table 2: Binding of Ligands to hXRCC1 at 25 °C in 50 mM Tris-HCl, pH 7.5, 100 mM NaCl, 5 mM $MgCl_2$, and 1 mM DTT[a]

ligand	K_d (nM)
1 nt-gapped DNA	34 ± 3
1 nt-gapped DNA (5′-P)[b]	52 ± 4
5 nt-gapped DNA	215 ± 10
nicked DNA	65 ± 5
duplex	230 ± 10
single-stranded oligonucleotide	260 ± 10

[a] K_d values (mean ± SE, $n = 3$) were determined by fluorescence titration. [b] 5′-P indicates the presence of a 5′-phosphate at the DNA terminus.

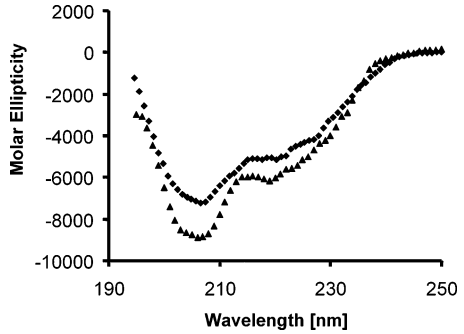

FIGURE 6: Far-UV CD spectrum of hXRCC1 (▲) and hXRCC1 + 10 μM 1 nt-gapped DNA (■). The concentration of hXRCC1 was 0.45 mg/mL in 50 mM Tris-HCl, pH 7.5, 100 mM NaCl, 5 mM $MgCl_2$, and 1 mM dithiothreitol.

of nicked DNA produced changes similar to those observed with gapped DNA in the CD spectrum of hXRCC1 (data not shown).

DISCUSSION

This study provides the first biophysical examination of full-length hXRCC1, a protein that plays an important role in base excision repair (BER) and single-strand break repair (SSBR) of damaged DNA. The hXRCC1 cDNA, which encodes a protein of 633 amino acids with a molecular mass of 69.5 kDa (*11*), was expressed in *E. coli*. However, the size of the purified recombinant protein as estimated by SDS−PAGE was 85 kDa, in agreement with the earlier reported values (*11*, *34*). This anomalous behavior in SDS−PAGE is not unique to XRCC1. Anomalous electrophoretic behavior has also been reported for several other proteins (*43*−*45*). For example, pig heart calpastatin with 713 amino acid residues (M_r 77122) exhibits an anomalous behavior in SDS gels, and the estimated molecular mass is 107 kDa (*43*). The observed slow migration in SDS gels could be a reflection of their unique amino acid compositions, being poor in aromatic acids and rich in proline and acidic residues. The proline content of XRCC1 is 9.5 mol %, and the acid residue content (Asp and Glu) is 14.3 mol %. This high content of negatively charged amino acids may restrict binding of SDS to hXRCC1, resulting in deviation from normal mobility expected for a protein of this size.

In the ultracentrifuge, the hXRCC1 sedimented with an intrinsic sedimentation coefficient, $s^0_{20,w}$, of 3.56, suggesting that it must be moderately asymmetric, since a globular protein like bovine serum albumin with a molecular mass of 66000 Da sediments much faster with an intrinsic sedimentation coefficient of 4.6. The sedimentation value decreased upon dilution, implying that the subunits are in a rapidly reversible equilibrium between monomeric and oligomeric forms. For a nonassociating system the *s* values should increase as the protein concentration decreases, since the frictional coefficient will decrease as the protein concentration is lowered. To understand the nature of the aggregation, sedimentation equilibrium experiments were carried out over a range of protein concentrations.

The self-association of hXRCC1 in 50 mM Tris-HCl, 0.10 M NaCl, 5 mM $MgCl_2$, and 2 mM dithiothreitol at pH 7.5 was characterized in detail. Sedimentation equilibrium studies demonstrated that hXRCC1 exists in a monomer−dimer equilibrium. The multiple sedimentation equilibrium data

sets, obtained at three initial loading concentrations as well as two rotor speeds, were fitted to a monomer−dimer model, and the K_a value of 1.75×10^6 M^{-1} indicates a strong association between monomers to form dimers. The association free energy (−8.5 kcal/mol) strongly favors dimer formation, such that at concentrations exceeding 0.6 mg/mL the reaction was nearly complete with 86% of the protein being dimerized. Zhang et al. (*17*) have determined the three-dimensional structure and fold of the C-terminal BRCT domain of hXRCC1. In the crystal structure there are two BRCT domains in the asymmetric unit forming a dimer. In the present study, we have demonstrated that intact hXRCC1 at higher concentrations can also exist as a dimer. It remains to be determined if hXRCC1 dimerization is mediated by its C-terminal BRCT domain. It is probable that the hXRCC1 C-terminal BRCT domain is also the site of interaction between full-length hXRCC1 and the complementary BRCT domain in DNA ligase III, because these two domains in truncated proteins have been shown to form a stable heterodimeric complex (*18*). Our finding that full-length XRCC1 protein in solution can also exist as a dimer suggests that the DNA ligase III binding site at the C-terminal BRCT domain in XRCC1 is conserved in the intact protein. Although XRCC1 tends to dimerize at higher concentrations, we believe that, under physiological conditions, XRCC1 will exist as a monomer in association with DNA ligase III. However, we still need to determine the relative amounts of both proteins in the cell and also determine their binding affinity and stoichiometry. The conserved BRCT domains in XRCC1 and other proteins enable them to dimerize, both within a single polypeptide and between different polypeptides, and there is evidence that these BRCT dimers facilitate phosphorylation-specific interactions and may have a regulatory role during repair (*46*, *47*).

Our finding that hXRCC1 is moderately asymmetric with the calculated dimensions of roughly 235 × 30 Å and an axial ratio of about 8:1, regardless of the model chosen, could have a bearing on its function. For a scaffolding protein capable of interacting with several proteins, it is advantageous to have an extended rodlike structure, thereby providing more surface area for other proteins to bind without much steric hindrance. Williams et al. (*48*) have predicted that proteins with more than two BRCT domains are likely to assume rodlike structures. Our data suggest that this prediction may be extended to proteins possessing two BRCT domains. At least four different proteins, PARP, DNA polymerase β, polynucleotide kinase, and DNA ligase III, in addition to XRCC1, are involved in recognizing and binding to radiation-induced single-strand break DNA. The scaffolding protein hXRCC1 may not only bring all the players together but may also regulate them (*12*, *49*). Defined regions of hXRCC1 are involved in binding these proteins. As mentioned, the N-terminal region is involved in binding DNA polymerase β, the C-terminal BRCT-II domain is responsible for binding to DNA ligase III and XRCC1 interacts with PARP through a central BRCT-I domain (*8*), and the linker region between the two BRCT domains which contains the CK2 phosphorylation sites interacts with the forkhead-associated domain of PNK (*23*).

The NMR solution structure of the XRCC1 N-terminal domain was studied in detail by Marintchev et al. (*20*). This domain specifically binds DNA with single-strand breaks (gapped and nicked), as evidenced by gel-shift assays (*20*). In the present study, we have determined the binding affinity and the stoichiometry of binding of these ligands to the full-length protein by fluorescence measurements, and these parameters are essential for understanding the role of hXRCC1. The binding was specific for 1 nt-gapped and nicked DNA, and the protein showed significantly lower affinities for the intact duplex with no break, a single-stranded oligonucleotide, and a 5 nt-gapped duplex. Our finding that hXRCC1 exhibits relatively low affinity toward a single-stranded oligonucleotide implies that recognition of single-strand breaks by hXRCC1 is intrinsic to the nature of the single-strand break itself, rather than the single strandedness that might occur through DNA breathing at the break site. Furthermore, the fact that a gap of five nucleotides causes a marked reduction in binding affinity suggests that XRCC1 contacts both the 3′ and 5′ termini of the strand break and this gap has to be <5 nucleotides for optimum binding.

The fact that hXRCC1 itself has high affinity (K_d values in the nanomolar range) for single-strand break DNA suggests that it could have a sensor function by itself. Current models of SSBR propose that PARP-1 functions as the primary single-strand break sensor (*50*). Arrival of XRCC1 at these PARP-bound sites may lead to an exchange of XRCC1 for PARP, with XRCC1 then functioning as a scaffolding protein directing the enzymes that carry out repair (*8*, *12*). However, the absence of PARP-1 does not prevent SSBR but only reduces the rate of repair 2−3-fold (*51*). In these circumstances XRCC1 may be acting as the strand break sensor in addition to its structural function.

Now that we have obtained some basic physical parameters for hXRCC1, it will be important to study in detail the mode of interaction of hXRCC1 with other proteins involved in single-strand break binding and repair. A similar approach using fluorescence spectroscopy and circular dichroism measurements should now allow us to examine binary, ternary, and quaternary complexes of these proteins.

ACKNOWLEDGMENT

We thank Emmanuel Guigard of the Biochemistry Department (University of Alberta) for sedimentation studies, Wayne Moffat, Spectral Services Supervisor, Department of Chemistry (University of Alberta), for CD analysis, and Dr. J. N. Mark Glover, Department of Biochemistry (University of Alberta), for valuable discussions.

REFERENCES

1. Thompson, L. H., Brookman, K. W., Jones, N. J., Allen, S. A., and Carrano, A. V. (1990) Molecular cloning of the human XRCC1 gene, which corrects defective DNA strand break repair and sister chromatid exchange, *Mol. Cell. Biol. 10*, 6160−6171.
2. Tebbs, R. S., Flannery, M. L., Meneses, J. J., Hartmann, A., Tucker, J. D., Thompson, L. H., Cleaver, J. E., and Pedersen, R. A. (1999) Requirement for the Xrcc1 DNA base excision repair gene during early mouse development, *Dev. Biol. 208*, 513−529.
3. Caldecott, K. W. (2003) XRCC1 and DNA strand break repair, *DNA Repair (Amsterdam) 2*, 955−969.
4. Thompson, L. H., and West, M. G. (2000) XRCC1 keeps DNA from getting stranded, *Mutat. Res. 459*, 1−18.
5. Tew, K. D., Colvin, O. M., and Chabner, B. A. (2001) Alkylating Agents, in *Cancer Chemotherapy and Biotherapy: Principles and Practices* (Chabner, B. A., and Longo, D. L., Ed.) pp 373−414, Lippincott Williams and Wilkins, Philadelphia, PA.
6. Moore, D. J., Taylor, R. M., Clements, P., and Caldecott, K. W. (2000) Mutation of a BRCT domain selectively disrupts DNA

single-strand break repair in noncycling Chinese hamster ovary cells, *Proc. Natl. Acad. Sci. U.S.A. 97*, 13649−13654.
7. El-Khamisy, S. F., Masutani, M., Suzuki, H., and Caldecott, K. W. (2003) A requirement for PARP-1 for the assembly or stability of XRCC1 nuclear foci at sites of oxidative DNA damage, *Nucleic Acids Res. 31*, 5526−5533.
8. Masson, M., Niedergang, C., Schreiber, V., Muller, S., Menissier-de Murcia, J., and de Murcia, G. (1998) XRCC1 is specifically associated with poly(ADP-ribose) polymerase and negatively regulates its activity following DNA damage, *Mol. Cell. Biol. 18*, 3563−3571.
9. Caldecott, K. W., Aoufouchi, S., Johnson, P., and Shall, S. (1996) XRCC1 polypeptide interacts with DNA polymerase beta and possibly poly (ADP-ribose) polymerase, and DNA ligase III is a novel molecular "nick-sensor" in vitro, *Nucleic Acids Res. 24*, 4387−4394.
10. Kubota, Y., Nash, R. A., Klungland, A., Schar, P., Barnes, D. E., and Lindahl, T. (1996) Reconstitution of DNA base excision-repair with purified human proteins: interaction between DNA polymerase beta and the XRCC1 protein, *EMBO J. 15*, 6662−6670.
11. Caldecott, K. W., McKeown, C. K., Tucker, J. D., Ljungquist, S., and Thompson, L. H. (1994) An interaction between the mammalian DNA repair protein XRCC1 and DNA ligase III, *Mol. Cell. Biol. 14*, 68−76.
12. Whitehouse, C. J., Taylor, R. M., Thistlethwaite, A., Zhang, H., Karimi-Busheri, F., Lasko, D. D., Weinfeld, M., and Caldecott, K. W. (2001) XRCC1 stimulates human polynucleotide kinase activity at damaged DNA termini and accelerates DNA single-strand break repair, *Cell 104*, 107−117.
13. Vidal, A. E., Boiteux, S., Hickson, I. D., and Radicella, J. P. (2001) XRCC1 coordinates the initial and late stages of DNA abasic site repair through protein−protein interactions, *EMBO J. 20*, 6530−6539.
14. Fan, J., Otterlei, M., Wong, H. K., Tomkinson, A. E., and Wilson, D. M., III (2004) XRCC1 co-localizes and physically interacts with PCNA, *Nucleic Acids Res. 32*, 2193−2201.
15. Bork, P., Hofmann, K., Bucher, P., Neuwald, A. F., Altschul, S. F., and Koonin, E. V. (1997) A superfamily of conserved domains in DNA damage-responsive cell cycle checkpoint proteins, *FASEB J. 11*, 68−76.
16. Callebaut, I., and Mornon, J. P. (1997) From BRCA1 to RAP1: a widespread BRCT module closely associated with DNA repair, *FEBS Lett. 400*, 25−30.
17. Zhang, X., Morera, S., Bates, P. A., Whitehead, P. C., Coffer, A. I., Hainbucher, K., Nash, R. A., Sternberg, M. J., Lindahl, T., and Freemont, P. S. (1998) Structure of an XRCC1 BRCT domain: a new protein−protein interaction module, *EMBO J. 17*, 6404−6411.
18. Nash, R. A., Caldecott, K. W., Barnes, D. E., and Lindahl, T. (1997) XRCC1 protein interacts with one of two distinct forms of DNA ligase III, *Biochemistry 36*, 5207−5211.
19. Taylor, R. M., Wickstead, B., Cronin, S., and Caldecott, K. W. (1998) Role of a BRCT domain in the interaction of DNA ligase III-alpha with the DNA repair protein XRCC1, *Curr. Biol. 8*, 877−880.
20. Marintchev, A., Mullen, M. A., Maciejewski, M. W., Pan, B., Gryk, M. R., and Mullen, G. P. (1999) Solution structure of the single-strand break repair protein XRCC1 N-terminal domain, *Nat. Struct. Biol. 6*, 884−893.
21. Marsin, S., Vidal, A. E., Sossou, M., Menissier-de Murcia, J., Le Page, F., Boiteux, S., de Murcia, G., and Radicella, J. P. (2003) Role of XRCC1 in the coordination and stimulation of oxidative DNA damage repair initiated by the DNA glycosylase hOGG1, *J. Biol. Chem. 278*, 44068−44074.
22. Schreiber, V., Ame, J. C., Dolle, P., Schultz, I., Rinaldi, B., Fraulob, V., Menissier-de Murcia, J., and de Murcia, G. (2002) Poly(ADP-ribose) polymerase-2 (PARP-2) is required for efficient base excision DNA repair in association with PARP-1 and XRCC1, *J. Biol. Chem. 277*, 23028−23036.
23. Loizou, J. I., El-Khamisy, S. F., Zlatanou, A., Moore, D. J., Chan, D. W., Qin, J., Sarno, S., Meggio, F., Pinna, L. A., and Caldecott, K. W. (2004) The protein kinase CK2 facilitates repair of chromosomal DNA single-strand breaks, *Cell 117*, 17−28.
24. Caldecott, K. W., Tucker, J. D., Stanker, L. H., and Thompson, L. H. (1995) Characterization of the XRCC1-DNA ligase III complex in vitro and its absence from mutant hamster cells, *Nucleic Acids Res. 23*, 4836−4843.
25. Babul, J., and Stellwagen, E. (1969) Measurement of protein concentration with interferences optics, *Anal. Biochem. 28*, 216−221.
26. Laue, T. M., and Stafford, W. F. (1999) Modern applications of analytical ultracentrifugation, *Annu. Rev. Biophys. Biomol. Struct. 28*, 75−100.
27. Williams, J. W., Van Holde, K. E., Baldwin, R. L., and Fujita, H. (1958) *Chem. Rev. 58*, 715−806.
28. Laue, T. M., Shah, B. D., Ridgeway, T. M., and Pelletier, S. L. (1991) in *Analytical Ultracentrifugation in Biochemistry and Polymer Science* (Harding, S. E., Rowe, A. J., and Horton, J. C., Eds.) pp 90−125, Royal Society of Chemistry, Cambridge, U.K.
29. Johnson, M. L., Correia, J. J., Yphantis, D. A., and Halvorson, H. R. (1981) Analysis of data from the analytical ultracentrifuge by nonlinear least-squares techniques, *Biophys. J. 36*, 575−588.
30. Cohn, E. J., and Edsall, J. T. (1943) in *Proteins* (Cohn, E. J., and Edsall, J. T., Eds.) pp 370−381, Reinhold Publishing Corp., New York.
31. Mani, R. S., and Kay, C. M. (1984) Hydrodynamic properties of bovine brain S-100 proteins, *FEBS Lett. 166*, 258−262.
32. Kuntz, I. D., Jr., and Kauzmann, W. (1974) Hydration of proteins and polypeptides, *Adv. Protein Chem. 28*, 239−345.
33. Compton, L. A., and Johnson, W. C., Jr. (1986) Analysis of protein circular dichroism spectra for secondary structure using a simple matrix multiplication, *Anal. Biochem. 155*, 155−167.
34. Pushnova, E. A., Ostanin, K., and Thelen, M. P. (2001) Human XPA and XRCC1 DNA repair proteins expressed in yeast, *Saccharomyces cerevisiae*, *Mol. Genet. Metab. 74*, 380−384.
35. Cann, J. R. (1970) *Interacting Macromolecules: the Theory and Practice of Their Electrophoresis, Ultracentrifugation, and Chromatography*, Academic Press, New York.
36. Zimmerman, J. K., and Ackers, G. K. (1971) Molecular sieve studies of interacting protein systems. VI. Effects of axial dispersion on boundary profiles of associating macromolecules, *J. Biol. Chem. 246*, 1078−1087.
37. Zimmerman, J. K., Cox, D. J., and Ackers, G. K. (1971) Molecular sieve studies of interacting protein systems. IX. Reaction boundary profiles for monomer-n-mer systems: comparison with sedimentation, *J. Biol. Chem. 246*, 4242−4250.
38. Hesterberg, L. K., and Lee, J. C. (1981) Self-association of rabbit muscle phosphofructokinase at pH 7.0: stoichiometry, *Biochemistry 20*, 2974−2980.
39. Erijman, L., and Weber, G. (1991) Oligomeric protein associations: transition from stochastic to deterministic equilibrium, *Biochemistry 30*, 1595−1599.
40. Schachman, H. K. (1959) *Ultracentrifugation in Biochemistry*, p 239, Academic Press, New York.
41. Tanford, C. (1961) *Physical Chemistry of Macromolecules.*, pp 196, 327, and 432, John Wiley and Sons, New York.
42. Van Holde, K. E. (1985) *Physical Biochemistry*, p 60, Prentice-Hall, Englewood Cliffs, NJ.
43. Takano, E., Maki, M., Mori, H., Hatanaka, M., Marti, T., Titani, K., Kannagi, R., Ooi, T., and Murachi, T. (1988) Pig heart calpastatin: identification of repetitive domain structures and anomalous behavior in polyacrylamide gel electrophoresis, *Biochemistry 27*, 1964−1972.
44. Yoshikawa, M., Mizukami, T., Omori, K., Sasaki, R., and Chiba, H. (1981) Isolation and characterization of messenger-RNA from mammary-gland of lactating cow, *Agric. Biol. Chem. 45*, 177−183.
45. Iino, T., Takeuchi, H., Nam, S. H., Siomi, H., Sabe, H., Kobayashi, N., and Hatanaka, M. (1986) Structural analysis of p28 adult T-cell leukaemia-associated antigen, *J. Gen. Virol. 67*, 1373−1379.
46. Caldecott, K. W. (2003) Cell signaling. The BRCT domain: signaling with friends?, *Science 302*, 579−580.
47. Manke, I. A., Lowery, D. M., Nguyen, A., and Yaffe, M. B. (2003) BRCT repeats as phosphopeptide-binding modules involved in protein targeting, *Science 302*, 636−639.
48. Williams, R. S., Green, R., and Glover, J. N. (2001) Crystal structure of the BRCT repeat region from the breast cancer-associated protein BRCA1, *Nat. Struct. Biol. 8*, 838−842.
49. Mitra, S., Izumi, T., Boldogh, I., Bhakat, K. K., Hill, J. W., and Hazra, T. K. (2002) Choreography of oxidative damage repair in mammalian genomes, *Free Radical Biol. Med. 33*, 15−28.
50. D'Silva, I., Pelletier, J. D., Lagueux, J., D'Amours, D., Chaudhry, M. A., Weinfeld, M., Lees-Miller, S. P., and Poirier, G. G. (1999) Relative affinities of poly(ADP-ribose) polymerase and DNA-

dependent protein kinase for DNA strand interruptions, *Biochim. Biophys. Acta 1430*, 119−126.
51. Sanderson, R. J., and Lindahl, T. (2002) Down-regulation of DNA repair synthesis at DNA single-strand interruptions in poly(ADP-ribose) polymerase-1 deficient murine cell extracts, *DNA Repair (Amsterdam) 1*, 547−558.
52. Chipman, D. M., Grisaro, V., and Sharon, N. (1967) The binding of oligosaccharides containing *N*-acetylglucosamine and *N*-acetylmuramic acid to lysozyme. The specificity of binding subsites, *J. Biol. Chem. 242*, 4388−4394.

BI048615M